Advanced Physical Research
Vol.6, No.2, 2024, pp.
https://doi.org/10.62476/

TUNNELING EFFECT IN DOUBLE QUANTUM DOTS NANOSTRUCTURE

Wisam Rysan[1], Fatima Rabeea JeJi[2], Baqer Obeid Al-Nashy[3*], Younis Mohamed Adiah Al-zahy[1]

[1]Department of Physics, College of Education, University of Misan, Maysan, Iraq
[2]Department of Physics, College of Education of Pure Science, Nassiriya Thi-Qar University, Thi-Qar, Iraq
[3]Department of Physics, College of Science, University of Misan, Maysan, Iraq

Abstract. In this working, we introduce a Q-DD composed of two QDs. We find that the absorption and dispersion spectra of the light pulse can be changed via the effect of and inter-dot tunnel couplings and probe pumping field of QDs. Then, we employ the steady state and dynamical state in the four-level double QDs system. The slope of dispersion switches from positive to negative. Therefore, both superluminal and Subluminal light propagations can be achieved by simply applying a gate voltage to the double inter dot tunnel coupling. It is also demonstrated that by applying the indirect pump probe field to the probe transition the absorption-free superluminal light propagation is obtained. The results show that by proper tuning of the bias voltage. This structure also indicates that a wide range of linearity from negative to positive can be simply adjusted via a bias voltage, which would result in wide control of signal beam.

Keywords: *Tunneling couplings, quantum double dot, Subluminal, superluminal.*

Corresponding Author: *Baqer Obeid Al-Nashy, Department of Physics, College of Science, University of Misan, Maysan, Iraq, e-mail: baqernano@uomisan.edu.iq*

Received: *25 March 2024;* ***Accepted:*** *22 April 2024;* ***Published:***

1. Introduction

The optical properties of quantum wells and quantum dots (QDs) to improve from through the external field and inter-dot tunnel coupling (Hao *et al*., 2012). Coherence induced by incoherent field and inter-dot tunnel coupling in the QDs system plays an important role in light–matter interaction and has found numerous implementations in semiconductor optics. On the other hand, coherent control (She *et al*., 2013; Nick Vamivakas *et al*., 2009; Vafafard *et al*., 2013; Al-Nashy & Al-Khursan, 2010; Asadpour *et al*., 2011) over the dispersive and absorptive properties of solid-state media such as photonic crystals and semiconductors has recently attracted a lot of attention (Niu *et al*., 2004; Kang & Zhu, 2003). Chemical Physical-properties of nanoparticles include size distribution, particle shape, size, solubility, purity, aggregation, porosity and agglomeration state, composition, surface chemistry, surface area and other characteristics that provide great information on nano-scale structure and could be

How to cite (APA):
Rysan, W., Rabeea JeJi, F., Al-Nashy, B.O. & Al-zahy, Y.M.A. (2024). Tunneling effect in double quantum dots nanostructure. *Advanced Physical Research, 6*(2),

dissimilar from the structures in the range of micrometer scale (Jabber Al-Saady *et al*., 2022).

Light–matter interaction plays an important role of system Coherence induced by incoherent field and inter-dot tunnel coupling in the QDs in and has found numerous implementations in semiconductor materials (Jabber Al-Saady *et al*., 2022; Kou *et al*., 2010; Matsko *et al*., 2003).

Recently as nanotechnology has more important role because it increases the capability to the atomic and molecular states (She *et al*., 2013). Nanoparticles have unique bio-physical and bio-chemical features (Ali *et al*., 2022).

Consider a three-level Y-type configuration in a QD system. This can be found in a QD molecule, as in Figure 1 which depicts a double QD with two conduction band levels apiece. The intersubband transitions are easily done theoretical. The subbands' configuration has two subsystems (Jiang & Zhu, 2008).

In the interaction picture, by using the rotating wave approximation (Jiang & Zhu, 2008), the semiclassical Hamiltonian of the system is given by Equation 1. Because the effect of the electron-electron interactions are expected to be rather weak in the present analysis, many body effects arising from electron-electron interactions are not included in our study (Mahmoudi & Sahrai, 2009; Al-Khursan *et al*., 2009).

In this work, interesting possibilities are explored, wherein the structure returns to a simple two-level system in many of the discussed cases. Their manufacture imperfections, the QDs have a nonuniformity in shape and size distribution (She *et al*., 2013; Hao *et al*., 2012; Vafafard *et al*., 2013; Sahrai *et al*., 2014; Kim & Chuang, 2006). Additionally the benefit of our structure here is a high value that cannot be obtained with any other real, simple two-level system. This results from the collective work of the three fields. Inclusion of inhomogenous broadening is shown in order to best demonstrate the experimental results of gain and refractive index (Hao *et al*., 2012).

The working is organized as follows: in Section 2, we present the theory model and obtain the density-matrix equations of motion for the system. In Section 3, we discuss the effects of incoherent pumping field and inter-dot tunnel couplings of QDs on probe detuning dispersion and absorption. We finally conclude in Section 4.

2. Theory model and equations

Using the density matrix approach for our system, shown in Figure 1 and under the rotating-wave and electric-dipole approximations, the time evolution of the system, expressed by the density operator ρ, leads to the following system of equations for the density matrix elements ρ_{ij}: Consider a QD molecule consisting of a two-QD (the right to left and one) system coupled by tunneling. As a realistic example, the asymmetric QD molecules have been detected in double layer InAs/GaAs structures (Nick Vamivakas *et al*., 2009) the density matrix equation of motion can be written as**,** under the rotating-wave approximation (Hamedi *et al*., 2013). Such a QD molecule can be fabricated using the self-assembled dot growth technology.

$$\dot{\rho}_{00}= \gamma_0\rho_{00}+i[T_{10}(\rho_{10}- \rho_{01})+\Omega_{20}(\rho_{20}- \rho_{02})+A_{03}(\rho_{30}- \rho_{03})+A_{04}(\rho_{40}- \rho_{04})$$
$$\dot{\rho}_{11}=- \gamma_1\rho_{11}+i[T_{10}(\rho_{01}- \rho_{10})+A_{12}(\rho_{21}- \rho_{12})+\Omega_{13}(\rho_{31}- \rho_{13})+A_{14}(\rho_{41}- \rho_{14})$$
$$\dot{\rho}_{22}=- \gamma_2\rho_{22}+i[\Omega_{20}(\rho_{02}- \rho_{20})+A_{12}(\rho_{12}- \rho_{21})+ T_{23}(\rho_{32}- \rho_{23})+A_{25}(\rho_{52}- \rho_{25})$$
$$\dot{\rho}_{33}= -(\gamma_3+ \gamma_2)\rho_{21}+i[\Omega_{31} (\rho_{33}- \rho_{22})+ T_{23}\rho_{31} +\Omega_{20}\rho_{01}+A_{25}\rho_{51}- T_{10}\rho_{20}- \Omega_{30}\rho_{23}- \phi_1A_{14}\rho_{43}$$
$$\dot{\rho}_{10}= -(\gamma_1+ \gamma_0)\rho_{10}+iT_{10}(\rho_{00}- \rho_{11})+A_{12}\rho_{20}+\Omega_{13}\rho_{30}+A_{14}\rho_{40}- \Omega_{20}\rho_{12}+A_{30}\rho_{13+} \phi_1A_{40}\rho_{14}$$

$$\dot{\rho}_{20} = -[i\Delta_{20}+[(\gamma_0+\gamma_2)]\ \rho_{20}+ i\ [\Omega_{20}\ (\rho_{00}-\rho_{22})+(A_{21}\rho_{10}+ T_{23}\rho_{30}+A_{25}\ \rho_{50})- A_{30}\rho_{23}- \phi_1 T_{10}\rho_{21}$$
$$\dot{\rho}_{21} = -(\gamma_2+\gamma_1)\rho_{21}+i[\Omega_{21}\ (\rho_{11}-\rho_{22})+ T_{23}\rho_{31}+\Omega_{20}\rho_{01}+A_{25}\rho_{51}- T_{10}\rho_{20}- \Omega_{13}\rho_{23}- \phi_2 A_{14}\rho_{43}$$
$$\dot{\rho}_{30} = -[i\Delta_{20}+[(\gamma_{33}+\gamma_{22})]\ \rho_{20}+ i\ [\Omega_{20}\ (\rho_{33}-\rho_{22})+(A_{21}\rho_{31}+ T_{23}\rho_{30}+A_{25}\ \rho_{50})- A_{30}\rho_{23}- T_{10}\rho_{21}$$
$$\dot{\rho}_{31} = -(\gamma_3+\gamma_2)\rho_{21}+i[\Omega_{21}\ (\rho_{33}-\rho_{11})+ T_{23}\rho_{31}+\Omega_{20}\rho_{21}+A_{25}\rho_{51}- T_{10}\rho_{30}- \Omega_{13}\rho_{23}-A_{14}\rho_{43} \quad (1)$$

Two levels |0>and |1> are the lower valance and upper conducting band levels of the left QD, respectively. Level |2> is the excited conducting level of the second QD, as shown in Figure 1(a). It is assumed that the energy difference of two lower levels as well as that of two excited states is large and then their tunneling couplings can be ignored. By applying a gate voltage the level |2> gets closer to the level |1>, while the valance band levels have still a high energy difference. The system configuration after applying the gate voltage is shown in Figure 1(b). A weak tunable probe field of frequency op with Rabi-frequency $\Omega_k=E_p$Ѡ$/\hbar$ applies to the transition |0>→||1>. Here Y_{01} is the atomic dipole moment and E_p. The first-order effect is calculated from the probe transition coherence $\rho_{20}^{(1)}$. An analytical relationship can be obtained by taking the solution of the system equations (1) at steady state. After some (long) mathematical manipulations, one can get the following relationship:

$$\rho_{10}^{(1)} = [T^2_{01}(\rho_{22}-\rho_{11})+A^2_{12}\ (\rho_{33}-\rho_{00})+ \phi_1\ \Omega_{20}\ (\rho_{40}-\rho_{12})+_{30}(\rho_{22}-\rho_{11})]/[\ (\gamma_3+\gamma_2)-i\Delta_{20}+[(\gamma_0+\gamma_2+)-(\gamma_1+\gamma_0)+ T_{23}A_{14}]\ \rho_{20}+ [T^2_{01}(\rho_{11}-\rho_{22})+A^2_{12}\ (\rho_{00}-\rho_{11})+ \phi_2\ \Omega_{20}\ (\rho_{40}-\rho_{12})+A_{30}(\rho_{22}-\rho_{11})]/[\ (\gamma_3+\gamma_2)- \phi_2\ i\Delta_{20}+[(\gamma_0+\gamma_2+)-(\gamma_1+\gamma_0)\ \Delta_{20}+ T^2_{23}A_{14}]\ \rho_{20}+ [T^2_{01}(\rho_{22}-\rho_{00})+A^2_{12}\ (\rho_{22}-\rho_{11})\ \Delta_{20}+ \phi_3\ \Omega_{20}\ (\rho_{22}-\rho_{33})+A_{30}(\rho_{22}-\rho_{11})]/[\ (\gamma_0+\gamma_1)-i\Delta_{20}+[(\gamma_0+\gamma_1)\ \Delta_{20}-(\gamma_2+\gamma_0)+ T_{23}A_{14}]\ \rho_{30} \quad (2)$$

$$\chi^{(1)} = [(2N|\mu|^2)/(\varepsilon_o\hbar\Omega_{20})]\ \rho_{10}^{(1)} \quad (3)$$

where N is the atomic number density in the medium. Our formula differs from all previous calculations because of convolution the inhomogeneous density of states in QDs is then given by (Mahmoudi & Sahrai, 2009):

In QDs, dephasing broadening is the dominant contribution, in contrast to the atomic systems (Jabber Al-Saady *et al*., 2022). Note that γ_i is the total decay rate from subband (i) and includes both the lifetime broadening due to longitudinal phonon emission at low temperature and the dephasing broadening, which results from both acoustic phonon scattering and scattering from interface roughness.

The real and imaginary parts of $\chi^{(1)}$ correspond to the linear dispersion and absorption, respectively , ε_0 is the permittivity of free space ,where N is the atomic number density in the medium, $\rho_{10}^{(1)}$ is the first order of the density operator of the probe transition and Ω_{10} is the Rabi frequency of the probe field and $\hbar$ is the normalised Planks constant (Joshi, 2009; Chang-Hasnain *et al*., 2003).

So, the system consists of two subsystems, i.e., one y type and the other form Λ type. Levels 1, 2 and 3 are in a usual three-type configuration and level 0 together with levels 1 and 2 forms a three-level-type configuration. Such a QD molecule can be fabricated using the self-assembled dot growth technology (Hao *et al*., 2012). Consider a QD molecule consisting of a double-QD (the left and right one) system coupled by tunneling. We consider a three-level double configuration in an asymmetric quantum dot system as shown in Figure 1, which has been realized experimentally. As a realistic example, the asymmetric QD molecules have been detected in double layer InAs/GaAs structures (Jiang & Zhu, 2008).

A cycling field frequency *m* is coupled to the transition 1 to 0 with transition frequency 01 and has a Rabi frequency equal to $\Omega_k=E_k/d_{01}$. The description of the optically allowed transitions in this system is as follows. The transition 1 to 2 transition frequency Ω_{21} interacts with a weak probe field E_1 frequency 1 having Rabi frequency $\Omega_{21}=E_1/d_{12}$ (Mahmoudi & Sahrai, 2009). The decay constants from levels 2 to 1, 1 to 0, 0 to 1 and 2 to 1 are 3, 2, 0 and 1, respectively. A coupling field E_0 frequency Ω_0 drives the transition 0 to 2 with transition frequency 02 with a Rabi frequency of $\Omega_0 =E_0/d_{02}$ while a pumping field E_2 frequency Ω_2 is acting on transitions 2 and 3 with transition frequency Ω_{21} and has a Rabi frequency equal to $\Omega_{21} =E_2/d_{23}$ (Hao *et al*., 2008; Niu *et al*., 2005; Nick Vamivakas *et al*., 2009; Xu *et al*., 2007).

The first contribution is mainly due to longitudinal optical LO photon emission at low temperature and the other contribution comes from electron. The proposed three-level atomic system has been shown in Figure 1, where, γ_0, γ_1 and γ_2, are decay rates of corresponding levels, respectively. The decay constants in semiconductor quantum wells are comprised of a population decay contribution as well as a dephasing contribution. The first control field has been applied to $|0>*\leftrightarrow|1>*$ transition with frequency ν_2 and Rabi frequency $\Omega_p = d_{20}E_1/\bar{h}$, the probe field with frequency ν_p and Rabi frequency $\Omega_p = d_{10}E_P/\bar{h}$ is driving $|1>*\leftrightarrow|2>:*$ transition (She *et al*., 2013).

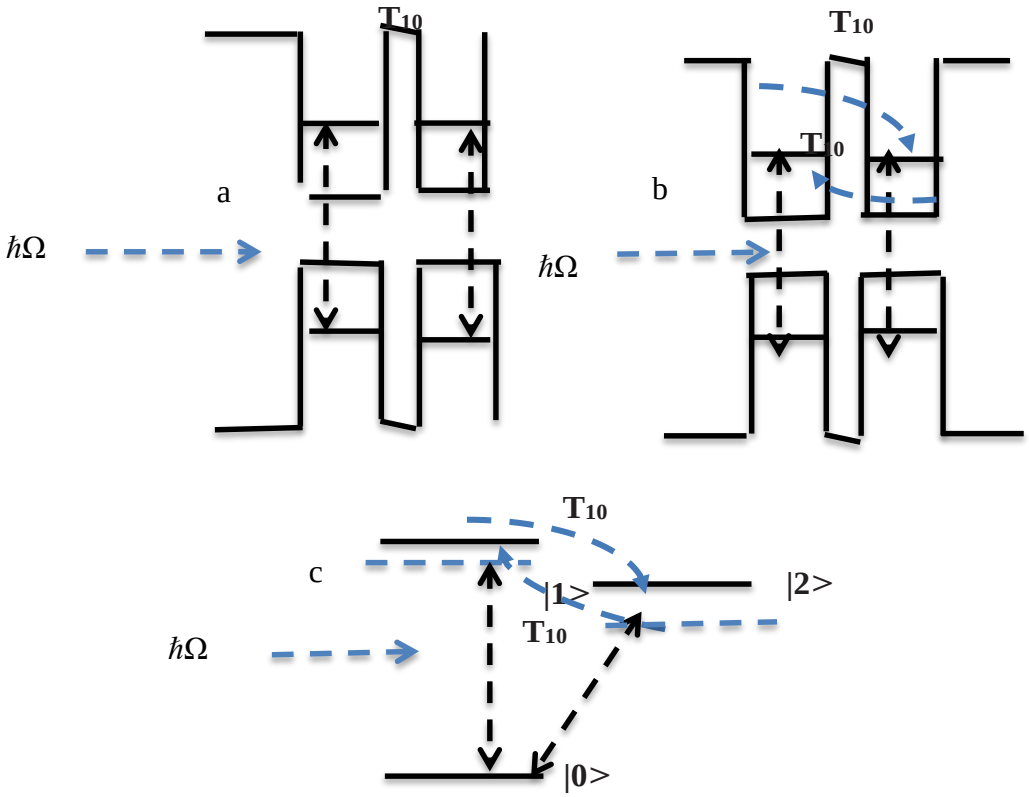

Figure 1. Schematic energy level diagram of a four-level system in Y-configuration. Here, $\omega_0(\Delta_0)$, $\omega_1(\Delta_1)$, $\omega_2(\Delta_2)$ and $\omega_m(\Delta_m)$ are frequencies (frequency detunings) of probe, cycling, coupling and pumping fields, respectively

The separation between the energies of the dark state and the remaining dressed atomic states of the Λ system is characterized by the total Rabi frequency $\Omega_k=\Omega_{01}+\Omega_{02}$. Assuming that the laser fields are tuned to the one- and two-photon resonances $\in_{01},\in_{21}$

$\ll \hbar\Omega$ the adiabatic approach holds if the off-diagonal matrix elements in equation (45) are much smaller than the total Rabi frequency Ω (Hao *et al*., 2012).

Energy-level diagram and excitation scheme of QD molecules system interacting with a strong control field (with half Rabi frequency W_c) and a weak probe optical field (with half Rabi frequency W_p). A bias voltage, which is added between two quantum dots, induces electron appearing tunneling effect and the corresponding tunneling strength is T_{10}. The detail description on the diagram sees the contexts of the paper (Vafafard *et al*., 2013).

3. Discussion and numerical results

To identify LWI, the first-order linear susceptibility was plotted in all the following figures. This assumption was also used in a large number of works, e.g. in (Hao *et al*., 2012) for the atomic system, in (Sahrai *et al*., 2014) for the quantum well system and in (Kim & Chuang, 2006) for the QD system.

The assumption of identical relaxation was used here ($\gamma_0 = \gamma_1 = \gamma_2 = \gamma_3 = 1$ meV) to simplify the calculations.

Figure 2 shows the first-order linear susceptibility as a function of normalised probe detuning Δ_0/γ_0 for the D-QD system. The following parameters are considered: $\Omega_{20} = -5\gamma$ and $\Omega_p = 0$, probe, pump, cycling and coupling, Rabi optical frequencies are, respectively.

Taking Figure 2 we are interested in the effect of interdot tunneling on the pulse propagation. This is a simple one photon pumping process. The slope of dispersion around zero detuning is negative, which corresponds to the superluminal light propagation and is accompanied by the absorption peak. We assume that a gate voltage is applied to the quantum molecule and induce the tunneling effect. The coherence in the system is created by coupling of two exciton states via tunneling instead of optical pumping (Xu *et al*., 2007). Note that in an atomic system the coherence is created by the laser field which is the main difference between these systems. Figure 2 shows the probe dispersion (a) and the absorption (b) in the presence of the tunneling effect. (a) As an example, when detuning $\Delta_{20}/\gamma_0 = 0.15$, the linear absorption is approximately zero, while $\chi^{(1)}$ reaches its maximum. Comparing Figure 2(a) with (c), if Ω_p is fixed. The quantum-dot has a base length of 9*nm* and a height of 3.5*nm* and an area density of about $4 \times 10^{-10} cm^2$ (Hao *et al*., 2012). Imaginary and real parts of the susceptibility as a function of Δ_k / γ_0 in plots (a)–(c) and as a function of Φ in plot (d). The other parameters are $\Delta_0 / \gamma_0 = \Delta_2 / \gamma_0 = \Delta_m / \gamma_0 = 0$, $\gamma_1 = \gamma_2 = \gamma_3 = 1.0$, $\gamma_0 = 0$, $\Omega_{01} / \gamma_0 = 0.005$, $\Omega_{01} / \gamma_0 = 0.5$, $\Omega_2 / \gamma_1 = 0.2$ and $\Omega_m / \gamma_1 = 0.5$. Plots (a), (b) and (c) are for $\Phi = 0, \pi / 3$ and $-\pi / 4$, respectively. For plot (d) we keep $\Delta_1 / \gamma_1 = 0$.

An investigation of Figure 3(a) shows that by introducing the tunneling effect the slope of dispersion around zero probe detuning switches from negative to positive corresponding to the light propagation. It also shows that by decreasing the tunneling parameter the slope of dispersion becomes steeper, corresponding to a stronger positive dispersion (Equation 2). Note that the slope of dispersion around $\Delta_m = 0$ is linear with respect to probe detuning. This is important for the pulse distortion during the propagation in a dispersive medium. If the real part of susceptibility has a linear slope, then in this spectral region, the pulse is not distorted during the propagation.

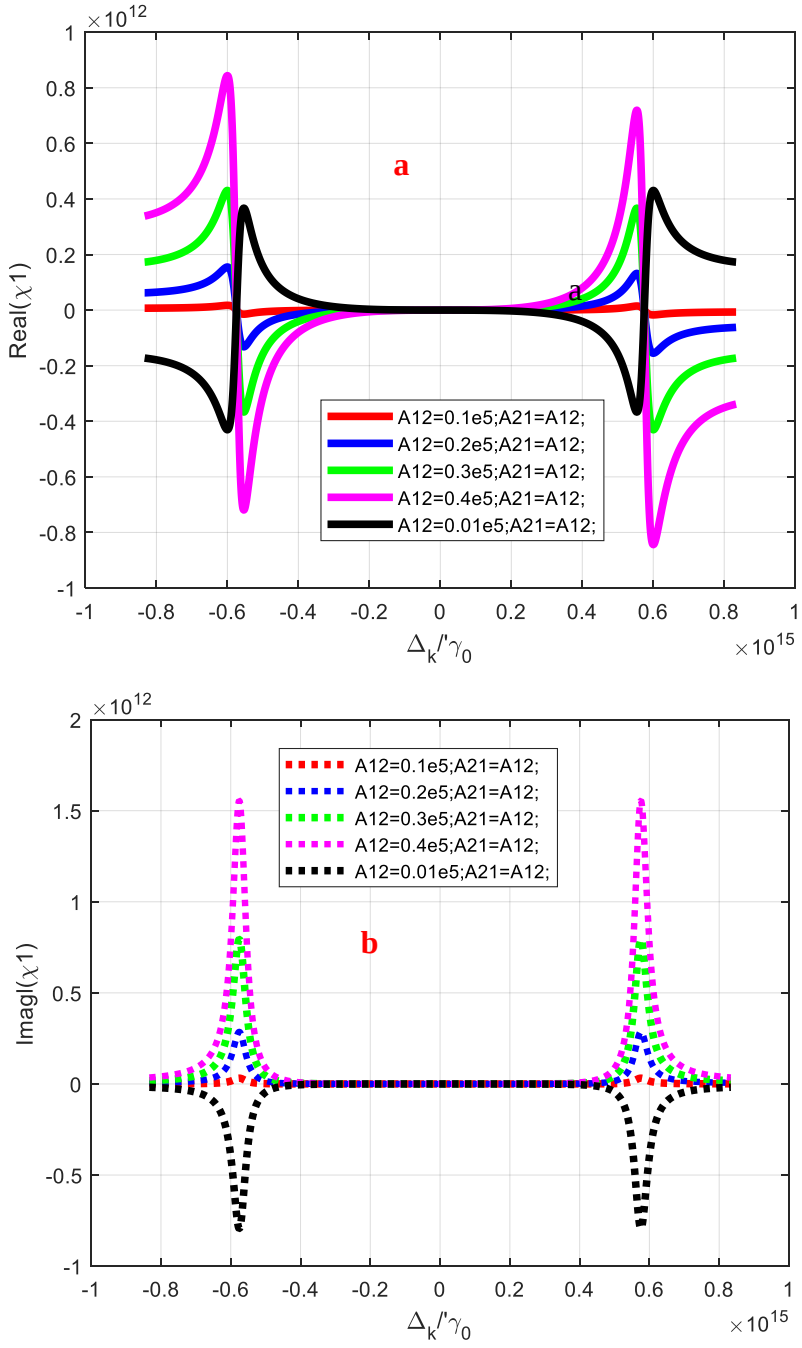

Figure 2. The real part and imaginary part of the linear optical susceptibility as a function of the detuning Δ_k/γ_0. The solid lines are real parts and the dashed lines are imaginary parts, linear absorption. Parameters are chosen as: $\gamma_{0=}1/\tau_0$, $\gamma_1=0/\tau_1$ $\gamma_2=1/\tau_{2,}$ $\gamma_3=1$, $\Omega_{21}=\Omega_{02}=\Omega_{01}=\Omega_{03}=\Omega_{13}=\Omega_k=0.364e15\gamma_0$eV, $\phi_1=\phi_2=\pi/3$ and $\phi_3=-\pi/4$, $\Delta_{01}=\Delta_{12}=1\gamma_0$, $\rho_{00}=\rho_{11}$ $\rho_{22}=\rho_{10=}\rho_{20}=1$, $T_{01}=T_{10}=0.03e5\gamma_0$, $A_{12}=A_{21}=0.1e5$, $\tau_0=0.12e\text{-}15$, $\tau_1=\tau_2=0.8e\text{-}10$

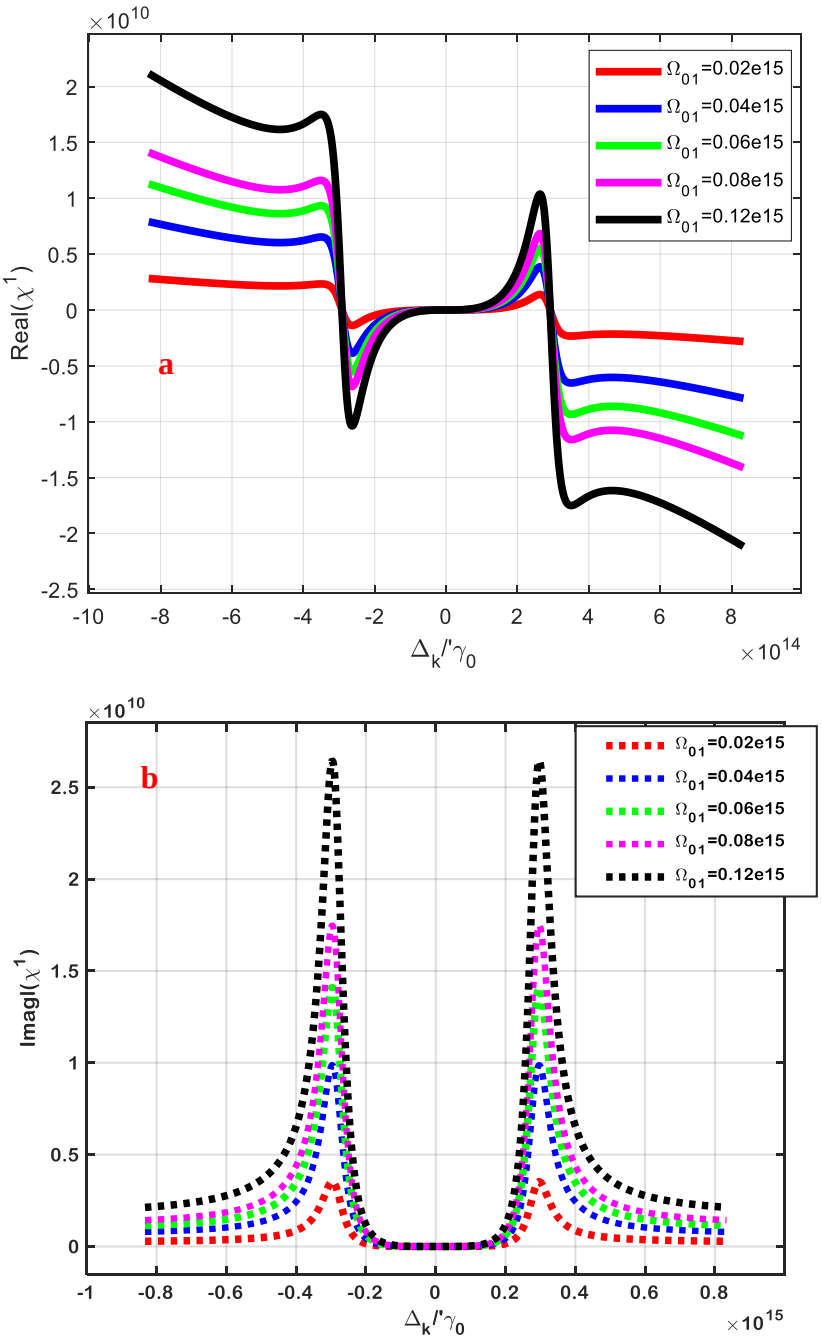

Figure 3. The real part and imaginary part of the linear optical susceptibility as a function of the detuning Δ_k/γ_0. The solid lines are real parts and the dashed lines are imaginary parts, linear absorption. Parameters are chosen as: $\gamma_0 = 1/\tau_0, \gamma_1 = 0/\tau_1 \ \gamma_2 = 1/\tau_2, \gamma_3 = 1$, $\Omega_{21} = \Omega_{02} = \Omega_{01,} = \Omega_{03} = \Omega_{13} = \Omega_k = 0.364e15\gamma_0$eV, $\phi_1 = \phi_2 = \pi/3$ and $\phi_3 = -\pi/4$, $\Delta_{01} = \Delta_{12} = 1\ \gamma_0$, $\rho_{00} = \rho_{11}\ \rho_{22} = \rho_{10} = \rho_{20} = 1$, $T_{01} = T_{10} = 0.03e5\gamma_0$, $A_{12} = A_{21} = 0.1e5$, $\tau_0 = 0.12e\text{-}15$, $\tau_1 = \tau_2 = 0.8e\text{-}10$

On the other hand, by taking into account the tunneling effect, the absorption doublet is appeared in the spectrum as shown in Figure 3(b) imaginary part of susceptibility and (b) real part of susceptibility vs. (a) Imaginary part of susceptibility and (b) real part of susceptibility vs. 1/; with parameters as, $\phi_p = \phi_2 = \phi_3 = 0$, 2 = Δ_m 1, Δ_m 3 = 0, ″Δ_m 2 = ″3 = (1, Ω_m 1.5, Ω_m 2, 2.5) × ″p. Δ_0/γ_1 Imaginary part of susceptibility and (b) real part of susceptibility vs. with parameters as, ϕp = ϕ2 = ϕ3 = 0, 2 = 0, 3 = 1,

″2 = ″3 = (1, 1.5, 2, 2.5) × Increasing $_m$ to 0.3γ changes the absorption into a gain with the appearance of the EIT window. Increasing the pump field to Ω_{01}= 0.7 γ_0 removes the EIT window and gives high gain. This result coincides with the conclusion in (Tarasov *et al*., 2021), where the EIT window is shown at low power Figure 4 linear susceptibility versus probe field detuning. (a) Linear absorption (dashed line) and dispersion (solid line). Imaginary and real parts of the susceptibility as a function of Δ_k/γ_0 in plots (a)–(b).

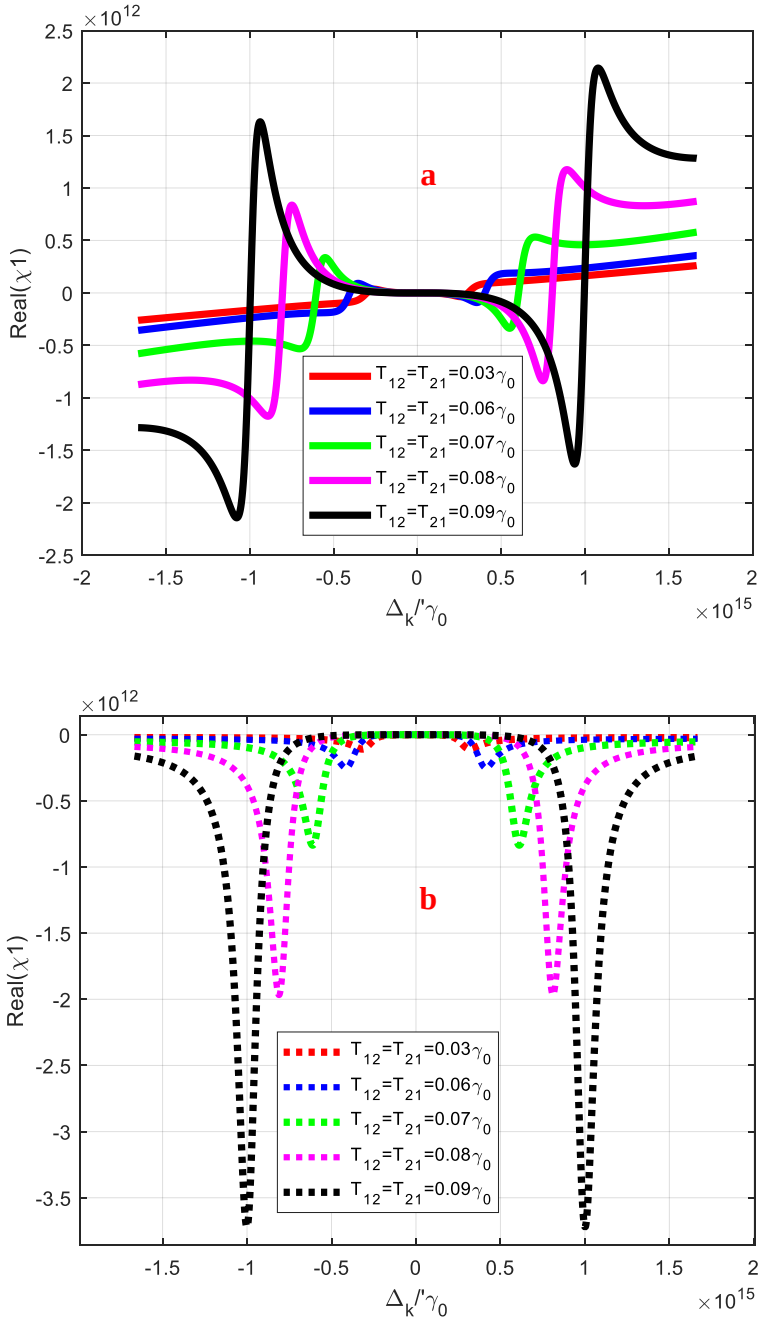

Figure 4. The real part and imaginary part of the linear optical susceptibility as a function of the detuning Δ_k/γ_0. The solid lines are real parts and the dashed lines are imaginary parts, linear absorption. Parameters are chosen as: γ_0=1/τ_0, γ_1 =0/τ_1 γ_2 =1/ τ_2, γ_3=0, Ω_{21}= Ω_{02} =Ω_{01}= Ω_{03}=Ω_{13}=Ω_k=0.364e15γ_0eV, ϕ_1= ϕ_2= π /3 and ϕ_3 =−π / 4, Δ_{01}= Δ_{12}=1 γ_0, ρ_{00}= ρ_{11} ρ_{22}= ρ_{10}= ρ_{20}=1, T_{01} = T_{10}=0.03e5γ_0, A_{12}=A_{21}=0.1e5, τ_0=0.12e-15, τ_1= τ_2=0.8e-10, respectively

The other parameters are γ_0=1/ τ_0, γ_1 =0/ τ_1 γ_2 =1/ τ_2, γ_3 = 0, Ω_1 / γ_1 = 0.364, Ω_0 / γ_1 = 0.5, Ω_2 / γ_1= 0.2 and Ω_m /γ_1 = 0.5. Plots (a), (b) and (c) are for ϕ_1 = ϕ_2 = π/3 and ϕ_3 =−π/4, respectively. For plot (d) we keep Δ_1 / γ_1 =0. Increasing the pump field to Δ_m = 0.7γ_0 removes the dispersion window and gives high gain. This result coincides with the conclusion in (Joshi, 2009), where the EIT window is shown at low power. Increasing Δ_m to 0.3γ changes the absorption into a gain with the appearance of the EIT window.

Figure 5 a high-resolution dispersion appears in the absorption spectrum due to the presence of tunnel coupling. The width of the dip is determined by Equation 6. By decreasing the tunneling parameter, the width of the dip is reduced. Note that for the selected parameters, the probe absorption Δ_m = 0 is negligible. The interesting region of the light propagation is a region that the system does not show the absorption or gain. This is due to the fact that the large absorption in the system does not permit the pulse propagates inside the medium. On the other hand, the gain also may add some noise to the system

Figure 5 optical susceptibility for Λ configuration (E_1 = 0) when (a) (Ω_0 = 0.01γ, Ω_2 = 0.1γ, Ω_m = 1.5γ), (Δ_1 = Δ_2 = Δ_m = 0); (b) (Ω_0 = 0.01γ, Ω_2 = 0.1γ, Ω_m = 1.5γ) and (Δ_1 =Δ_2 = Δ_m = 5γ) as a function of probe detuning, (Δ_k), normalized to the decay rate (γ_0); (c) as function of coupling field Rabi energy Ω_2. It is well known that the dispersion curves can be divided into normal and anomalous dispersion regimes.

It is also obvious that with changing the detuning D from -1.0 meV to 1.0 meV, the width of the left-hand side TW increases accompanied by decreasing that of the right-hand one (Figure 5 b).

The system parameters used are T_{01} = 2.0meV, k_{12} = 3.66 × 10^4cm^{-1}meV, A_{12} = 0.1meV, A_{13} = 0.2meV, g_2 = 1.0meV, Ω_{12} = 0.1meV and Ω_{13} = 1.0 × 10^{-3}meV. One sees that, when the detuning D increases, both the linear absorption and the dispersion curves standing in both side of the central angular frequencies w_p shift slight toward left, although the curves around the central angular frequencies have hardly changed.

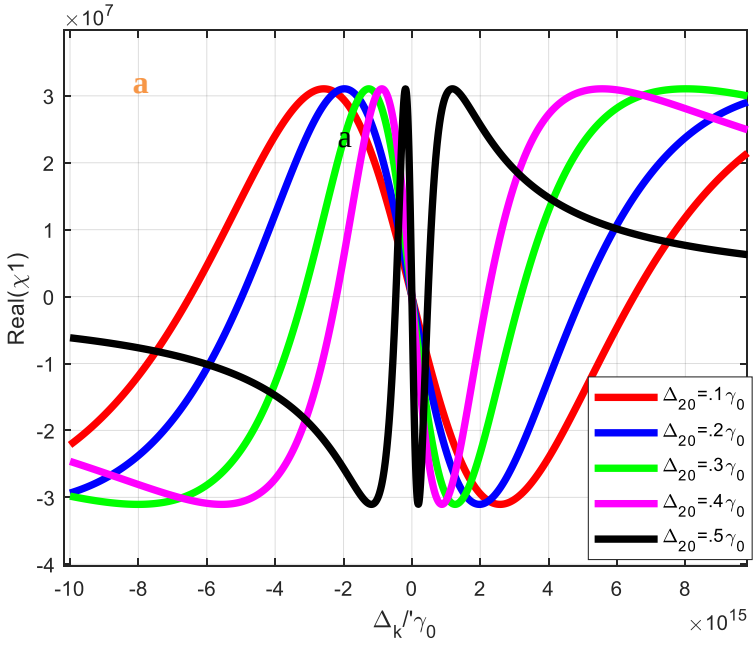

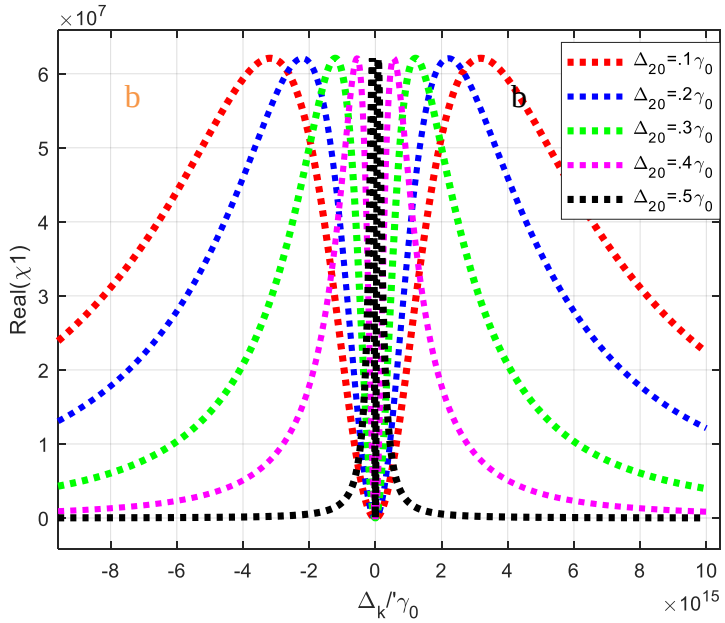

Figure 5. The real part and imaginary part of the linear optical susceptibility as a function of the detuning Δ_k/γ_0. The solid lines are real parts and the dashed lines are imaginary parts, linear absorption. Parameters are chosen as: γ_0=1/τ_0, γ_1 =0/τ_1 γ_2 =1/τ_2, γ_3=1, Ω_{21}=Ω_{02}=Ω_{01}= Ω_{03}=Ω_{13}=Ω_k=0.364e15γ_0eV, ϕ_1 = ϕ_2 = π/3 and ϕ_3 =−π / 4, Δ_{01}=Δ_{12}=1 γ_0, ρ_{00}=ρ_{11} ρ_{22}=ρ_{10}= ρ_{20}=1, T_{01} = T_{10}=0.03e5γ_0, A_{12}=A_{21}=0.1e5, τ_0=0.12e-15, τ_1= τ_2=0.8e-10, respectively

Figure 6 at the centre of the cycling field, the gain peak appears. When the system is probe-detuned, EIT was shown. Increasing probe detuning gives a wider EIT with a higher gain peak. Wide EIT is important in slow light applications (Hamedi *et al*., 2013). So, one can use the pumping field to switch between absorption and gain. Both gain and absorption are increased and blue shifted with an increase in probe detuning.

The behaviour under the effect of the pump field differs from that of the cycling field Ω_k shown in Figure 6, where the absorption peaks appear in the negative pump field frequencies and gain peaks appear in the positive pump field.

Optical susceptibility for weak probe-configuration (E_0 = 0) as a function of probe detuning, normalized to the decay rate (γ_0) when (a) (Ω_1 = 0.01γ, Ω_2 = 0.1γ, Ω_{21} = 1γ), (Δ_1 = Δ_2 = 0, Δ_k = 5γ); (b) as a function of phase in when (Ω_1 = 0.1γ, Ω_2 = 0.1γ, Ω_{10}= 1γ) and (Δ_0 = Δ_1= Δ_2= 0, Δ_2= 5γ). Note that (γ_0 = γ_1 = γ_2 = γ_3 = γ = 1 meV). When (Ω_0 = 0.01γ, Ω_m = 1γ) (Δ_0 = Δ_1=Δ_2 = 0, Δ_k = 3γ); (d) as a function of phase when (Ω_0= 0.01γ, Ω_2 = 0.1γ, Ω_k=γ), (Δ_0 = Δ_1 = 0, Δ_2 = 5γ, Δ_m= 0). Note that (γ_0 = γ_1 = γ_2 = γ_3 = γ = 1 meV). The probe detuning.

Figure 7(a) shows the case when the probe field is turned off. The structure is connected now with the coupling and pump fields. A negative and steep dispersion is obtained around zero detuning with a considerable linear gain. The EIT window with neglected linear gain peaks is shown. Figure 7(a) shows the phase control of the weak probe case of our structure.

Shows the same as in Figure 6, but here while Δ_2 = 0 increasing the pumping field to Δ_k = 5γ gives the gain (black and red curves) at Δ_1 = 0.5γ and γ and absorption at Δ_k = 5γ and 7γ (blue and green curves), both with the wide EIT window obtained for absorption. Figure 7 shows the effect of pump detuning (Δ_k) under Δ_1= 3γ_1, Δ_2 = 0. A complete gain spectrum with the EIT window under different pump detunings (Δ_k= 3γ,

5γ and 7γ) is obtained. A wide EIT window and reduction of gain were obtained at high pump detuning (Δ_k = 7γ) as shown by the green curve. Figure 7 shows the periodicity behavior of linear susceptibility under the phase effect with the pumping field as a variable parameter. The gain with small amplitude was obtained at the low pump (Δ_m = 0.3γ) as in the red.

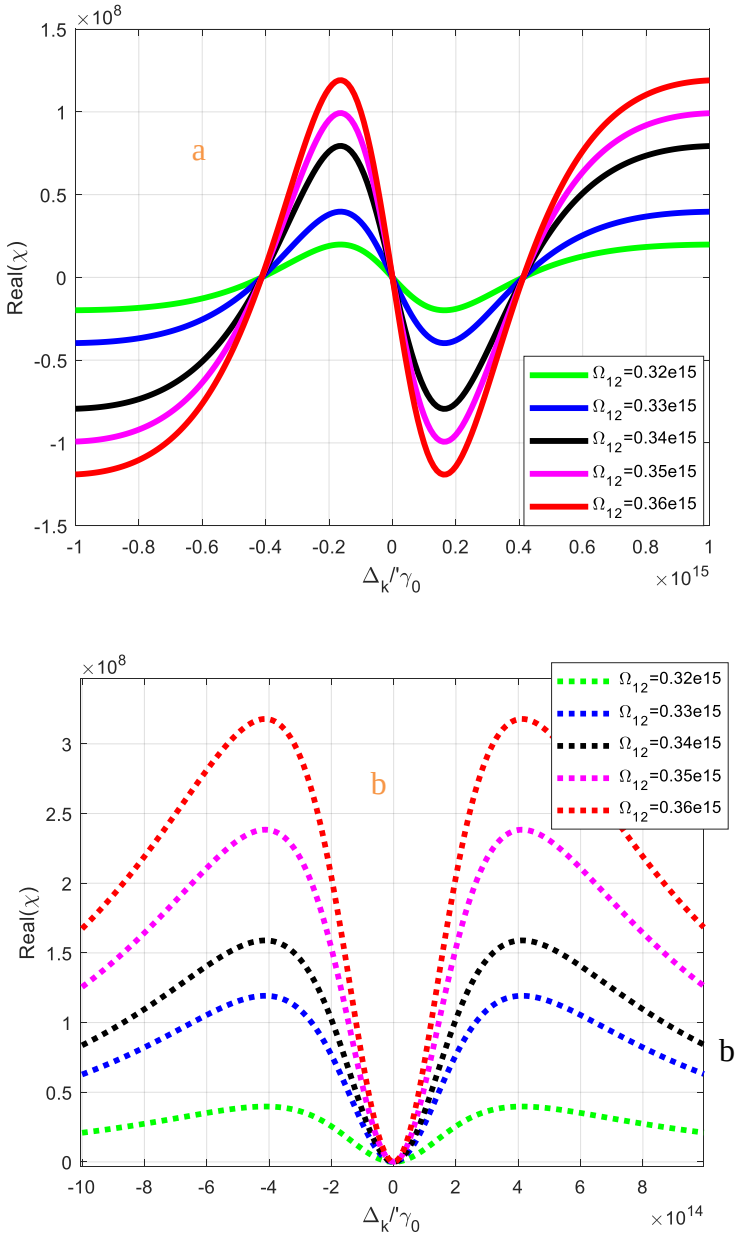

Figure 6. The real part and imaginary part of the linear optical susceptibility as a function of the detuning Δ_k/γ_0. The solid lines are real parts and the dashed lines are imaginary parts, linear absorption. Parameters are chosen as: γ_0=1/ τ_0, γ_1 =0/τ_1 γ_2 =1/τ_2, γ_3=1, Ω_{21}=Ω_{02}=Ω_{01}=Ω_{03} =Ω_{13}=Ω_k=0.364e15γ_0eV, ϕ_1 = ϕ_2 = π/3 and ϕ_3 =−π / 4, Δ_{01}= Δ_{12}=1 γ_0, ρ_{00}= ρ_{11} ρ_{22}= ρ_{10}= ρ_{20}=1, T_{01} = T_{10}=0.03e5γ_0, A_{12}= A_{21}=0.1e5, τ_0=0.12e-15, τ_1= τ_2=0.8e-10, respectively

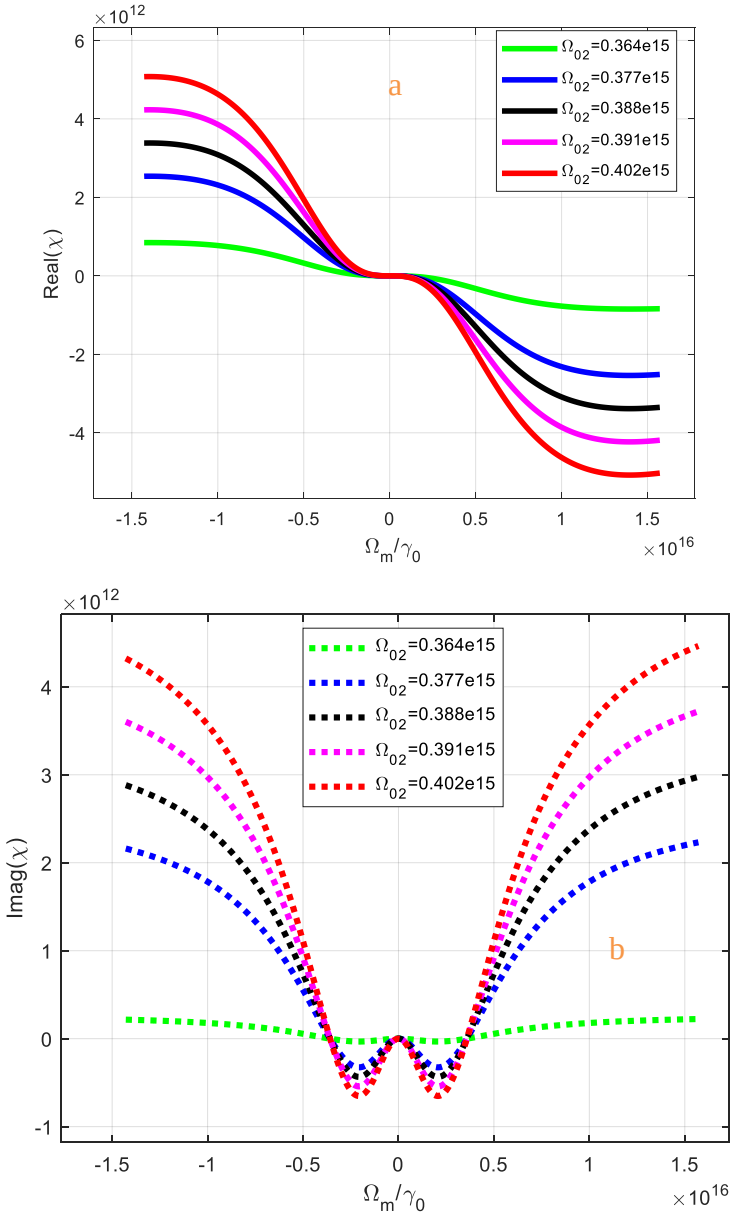

Figure 7. The real part and imaginary part of the linear optical susceptibility as a function of the detuning Δ_k/γ_0. The solid lines are real parts and the dashed lines are imaginary parts, linear absorption. Parameters are chosen as: γ_0=1/ τ_0, γ_1 =0/ τ_1 γ_2 =1/ τ_2, γ_3 = 1, Ω_{21}= Ω_{02} =Ω_{01}= Ω_{03} =Ω_{13}=Ω_k=0.364e15γ_0eV, ϕ_1 = ϕ_2 = π / 3 and ϕ_3 =−π / 4, Δ_{01} = Δ_{12}=1 γ_0, ρ_{00}= ρ_{11} ρ_{22}= ρ_{10}= ρ_{20}=1, T_{01} = T_{10}=0.03e5γ_0, A_{12}=A_{21}=0.1e5, τ_0=0.12e-15, τ_1= τ_2=0.8e-10, respectively

4. Conclusions

In conclusion, we investigated the absorption and dispersion of a weak pump probe field in a double quantum-dot. It was shown that by taking into account the double inter dot tunnel coupling, the slope of dispersion switches from positive to negative. Therefore, both superluminal and Subluminal light propagations can be achieved by simply applying a gate voltage to the double inter dot tunnel coupling. It is also demonstrated that by applying the indirect pump probe field to the probe transition the absorption-free superluminal light propagation is obtained. In

conclusion, we have theoretically investigated the enhancement of first order linearity in asymmetric double QDs. The results show that by proper tuning of the bias voltage.

References

Akram, H., Al-Khursan, A. H. (2016). Second-order nonlinearity in ladder-plus-Y configuration in double quantum dot structure. *Applied Optics*, *55*(34), 9866-9874.

Ali, Z.H., Al-Saady, M.A.A.J., Aldujaili, N.H., Rabeea Banoon, S. & Abboodi, A. (2022). Evaluation of the antibacterial inhibitory activity of chitosan nanoparticles biosynthesized by streptococcus thermophilus. *Journal of Nanostructures*, *12*(3), 675-685. https://doi.org/10.22052/JNS.2022.03.020

Al-Khursan, A.H., Al-Khakani, M.K. & Al-Mossawi, K.H. (2009). Third-order non-linear susceptibility in a three-level QD system. *Photonics and Nanostructures-Fundamentals and Applications*, *7*(3), 153-160.

Al-Nashy, B., Al-Khursan, A.H. (2010). Linear and nonlinear gain of SB-based quantum-dot semiconductor optical amplifiers. *Recent Patents on Electrical & Electronic Engineering (Formerly Recent Patents on Electrical Engineering)*, *3*(3), 232-240. https://www.researchgate.net/publication/284516550

Asadpour, S.H., Sahrai, M., Sadighi-Bonabi, R., Soltani, A. & Mahrami, H. (2011). Enhancement of Kerr nonlinearity at long wavelength in a quantum dot nanostructure. *Physica E: Low-dimensional Systems and Nanostructures*, *43*(10), 1759-1762.

Chang-Hasnain, C.J., Ku, P.C., Kim, J. & Chuang, S.L. (2003). Variable optical buffer using slow light in semiconductor nanostructures. *Proceedings of the IEEE*, *91*(11), 1884-1897.

Hamedi, H.R., Asadpour, S.H. & Sahrai, M. (2013). Giant Kerr nonlinearity in a four-level atomic medium. *Optik*, *124*(4), 366-370.

Hao, X., Wu, J. & Wang, Y. (2012). Steady-state absorption–dispersion properties and four-wave mixing process in a quantum dot nanostructure. *JOSA B*, *29*(3), 420-428.

Hao, X., Yang, W.X., Lü, X., Liu, J., Huang, P., Ding, C. & Yang, X. (2008). Polarization qubit phase gate in a coupled quantum-well nanostructure. *Physics Letters A*, *372*(47), 7081-7085.

Jabber Al-Saady, M.A.A., Aldujaili, N.H., Banoon, S.R. & Al-Abboodi, A. (2022). Antimicrobial properties of nanoparticles in biofilms. *Revis Bionatura*, *7*(4), 71. http://dx.doi.org/10.21931/RB/2022.07.04.71

Jiang, Y.W., Zhu, K.D. (2008). Controlling Kerr nonlinearity with electric fields in asymmetric double quantum-dots. *arXiv preprint arXiv:0801.3726*.

Joshi, A. (2009). Phase-dependent electromagnetically induced transparency and its dispersion properties in a four-level quantum well system. *Physical Review B*, *79*(11), 115315.

Kang, H., Zhu, Y. (2003). Observation of large Kerr nonlinearity at low light intensities. *Physical Review Letters*, *91*(9), 093601.

Kim, J., Chuang, S.L. (2006). Theoretical and experimental study of optical gain, refractive index change and linewidth enhancement factor of p-doped quantum-dot lasers. *IEEE Journal of Quantum Electronics*, *42*(9), 942-952.

Kou, J., Wan, R.G., Kang, Z.H., Wang, H.H., Jiang, L., Zhang, X.J. & Gao, J.Y. (2010). EIT-assisted large cross-Kerr nonlinearity in a four-level inverted-Y atomic system. *JOSA B*, *27*(10), 2035-2039.

Mahmoudi, M., Sahrai, M. (2009). Absorption-free superluminal light propagation in a quantum-dot molecule. *Physica E: Low-dimensional Systems and Nanostructures*, *41*(10), 1772-1778.

Matsko, A.B., Novikova, I., Welch, G.R. & Zubairy, M.S. (2003). Enhancement of Kerr nonlinearity by multiphoton coherence. *Optics Letters*, *28*(2), 96-98.

Nick Vamivakas, A., Zhao, Y., Lu, C.Y. & Atatüre, M. (2009). Spin-resolved quantum-dot

resonance fluorescence. *Nature Physics*, *5*(3), 198-202.

Niu, Y., Gong, S., Li, R. & Jin, S. (2004). Creation of atomic coherent superposition states via the technique of stimulated Raman adiabatic passage using a Λ-type system with a manifold of levels. *Physical Review A, 70*(2), 023805.

Niu, Y., Gong, S., Li, R., Xu, Z. & Liang, X. (2005). Giant Kerr nonlinearity induced by interacting dark resonances. *Optics Letters*, *30*(24), 3371-3373.

Sahrai, M., Mehmannavaz, M.R. & Sattari, H. (2014). Optically controllable switch for light propagation based on triple coupled quantum dots. *Applied Optics*, *53*(11), 2375-2383.

She, Y., Zheng, X., Wang, D. & Zhang, W. (2013). Controllable double tunneling induced transparency and solitons formation in a quantum dot molecule. *Optics Express*, *21*(14), 17392-17403.

Tarasov, G.G., Zhuchenko, Z.Y., Lisitsa, M.P., Mazur, Y.I., Wang, Z.M., Salamo, G.J. & Kissel, H. (2006). Optical detection of asymmetric quantum-dot molecules in double-layer InAs/GaAs structures. *Semiconductors*, 40, 79-83.

Vafafard, A., Goharshenasan, S., Nozari, N., Mortezapour, A. & Mahmoudi, M. (2013). Phase-dependent optical bistability in the quantum dot nanostructure molecules via inter-dot tunneling. *Journal of Luminescence*, 134, 900-905.

Xu, X., Sun, B., Berman, P.R., Steel, D.G., Bracker, A.S., Gammon, D. & Sham, L.J. (2007). Coherent optical spectroscopy of a strongly driven quantum dot. *Science*, *317*(5840), 929-932.